Biosensors and Bioelectronics 204 (2022) 114084

Contents lists available at ScienceDirect

Biosensors and Bioelectronics

journal homepage: www.elsevier.com/locate/bios

Optothermophoretic flipping method for biomolecule interaction enhancement

Jiajie Chen [a,*,1], Youjun Zeng [a,1], Jie Zhou [a], Xueliang Wang [a], Boliang Jia [a], Ruibiao Miyan [a], Teliang Zhang [a], Wei Sang [a], Ying Wang [b], Haixia Qiu [b], Junle Qu [a], Ho-Pui Ho [c], Bruce Zhi Gao [d], Yonghong Shao [a,**], Ying Gu [b]

[a] Key Laboratory of Optoelectronic Devices and Systems of Ministry of Education and Guangdong Province, College of Physics and Optoelectronics Engineering, Shenzhen University, Shenzhen, 518060, China
[b] Department of Laser Medicine, First Medical Center of PLA General Hospital, Beijing, 100853, China
[c] Department of Biomedical Engineering, The Chinese University of Hong Kong, Shatin, Hong Kong
[d] Department of Bioengineering and COMSET, Clemson University, Clemson, SC, 29634, USA

ARTICLE INFO

Keywords:
Surface plasmon resonance sensing
Optical manipulation
Molecule manipulation
Molecular interaction
Optofluidics

ABSTRACT

The widely used surface-based biomolecule sensing scheme has greatly facilitated the investigation of protein-protein interactions in lab-on-a-chip microfluidic systems. However, in most biosensing schemes, the interactions are driven in a passive way: The overall sensing time and sensitivity are totally dependent on the Brownian diffusion process, which has greatly hindered their efficiency, especially at low concentration levels or single-molecule analysis. To break this limitation, we developed an all-optical active method termed optothermophoretic flipping (OTF). It is the first temporal modulated method that biomolecules were enriched and pushed to their counterparts for effective contact via a flipped thermophoresis. As a proof-of-concept experiment, we tested its performance via antibody-antigen binding on a surface plasmon resonance imaging (SPRi) platform. Compared with the interaction solely based on Brownian diffusion, we achieved a 23.6-fold sensitivity increment in biomolecule interactions sensing. This method has opened new opportunities for various biosensing platforms that require high-sensitivity in colloidal sciences and biochemical studies.

1. Introduction

Proteins are vital components in a living organism; they play an important role in energy transportation, cell functioning, and immune response. The study of protein-protein interactions is a hot topic in the field of biosensing. Especially, antibody and antigen interactions are of great importance in point-of-care diagnosis(Brangel et al., 2018; Wang, 2006). Numerous biosensing schemes such as enzyme-linked immunosorbent assays (ELISA) (Ju et al., 1999; Lequin, 2005; Sun et al., 2001), Colorimetric assays (Song et al., 2011), material fluorescence (Li and Zhu, 2013; Zhang et al., 2011; Zhong, 2009), chemiluminescence assays (Dufour et al., 2003; Tanaka and Matsunaga, 2000), Raman spectroscopy (Chou et al., 2008; Henry et al., 2016; Laing et al., 2017; Tripp et al., 2008), and surface plasmon resonance (SPR) (Law et al., 2009; Mejía-Salazar and Oliveira Jr, 2018; Xin et al., 2018) biosensors have been developed to investigate the corresponding biochemical properties and behaviors. In particular, Xin et al. pioneered the optical detection of quantum biological electron transfer during different redox processes of protein within living cells based on an elegant SPR particle-based tunnel junction with high sensitivity and selectivity, which opens up a new set of molecular detection and imaging modality (Xin et al., 2019). Nevertheless, most of the biomolecular sensors are designed to act passively, i.e., the driving force for an effective interaction between target biomolecules is mainly dependent on their Brownian motion and diffusion process. Although some microstructures are designed to enhance the sensing event (Chen et al., 2017; Lynn et al., 2014), at low sample concentration level, the possibility of an effective collision for subsequent biomolecule binding becomes quite low, which inhibits subsequent sensing performance.

In the past decade, various kinds of active biosensing techniques

* Corresponding author.
** Corresponding author.
E-mail addresses: cjj@szu.edu.cn (J. Chen), shaoyh@szu.edu.cn (Y. Shao).
[1] These authors contributed equal to the article.

https://doi.org/10.1016/j.bios.2022.114084
Received 27 July 2021; Received in revised form 4 January 2022; Accepted 6 February 2022
Available online 11 February 2022

emerged. Generally, these schemes are primarily of two types: One is nanostructures with precise fabrication processes, and the other is the method to drive and enrich the solutes towards the vicinity of the sensing surface via different kinds of active external forces. For example, in 2011, a DNA sensing enhancement scheme was developed using superhydrophobic nanostructures for solute concentration; a sample of extremely low concentration (aM) can be detected after solvent evaporation(De Angelis et al., 2011). For liquid-based enhancement and manipulation schemes, acoustical (Liu et al., 2003; Ozcelik et al., 2018; Voiculescu and Nordin, 2012), electrical (Barik et al., 2017; Li et al., 2018; Liu et al., 2011), and optothermal effects (Fränzl et al., 2019; Garcia-Guirado et al., 2018; Hong et al., 2020; Karim et al., 2019; Kim et al., 2020), are the three most commonly used methods. Two aspects can serve as the standard to accessing the sensing enhancement level: One is sensing time reduction rate, and the other is the sensitivity increment rate. Recently, in 2018, an electro-thermo-plasmonic (ETP) effect enhancement scheme reached 2.9 × faster than the diffusion-limited case(Garcia-Guirado et al., 2018). In 2020, Y. Kim et al. proposed a bubble-mediated molecular concentration method to enrich the biomolecule to the border of the thermal induced bubble; they have achieved a sensitivity enhancement of 8.7 × (Kim et al., 2020). However, there still exists several issues about the intermolecular sensing enhancement. Firstly, most of the aforementioned sensing schemes provide the molecules to surface interaction enhancing, while the specific molecules to molecules interaction enhancement is rarely achieved. Secondly, the major optothermal diffusion-limited breaking methods still need the assistance of other forces such as electrical field or multi-phase interactions. Thirdly, for the existing sensing enhancement strategies, the sensing signal is in 1D, i.e., an integrated signal from the sensing area which lacks effective imaging ability to monitor the whole 2D sensing area in real time.

To address the above issues, we present a surface plasmon resonance imaging (SPRi) based temporal modulated optothermophoretic flipping (OTF) method for biomolecule interaction enhancement, and we have greatly enlarged the sensitivity enhancement to a factor up to 23.6. The SPRi is an emerging tool in recent years that offers label-free, real-time, and high sensitive sensing, and it can be extensively applied in biochemistry studies(Sereda et al., 2014; Wang et al., 2020; Yuk et al., 2004; Zeng et al., 2017; Zhou et al., 2020). Here, we adopt the wavelength based SPRi (WSPRi) as our sensing platform, the WSPRi can provide us a hyperspectral image of resonance wavelength of SPR, i.e., each pixel on the image of the sensing surface serves as an independent sensing unit to obtain its own SPR spectrum(Liedberg et al., 1993; Wu et al., 2018; Zeng et al., 2019). This can provide not only intermolecular interaction information in multiple sensing sites, but also a high throughput of signal detection(Chen et al., 2016b; Zeng et al. 2016, 2020). In addition, the OTF method is based on thermophoretic force exerted on biomolecules or nanoparticles induced by temperature gradient (Eslahian et al., 2014; Jiang et al., 2020; Lüsebrink et al., 2012; Reichl et al., 2014; Vigolo et al., 2010), which has drawn great attention in the study of biological problems(Braun and Cichos, 2013; Chen et al., 2016a; Cong et al., 2018; Ding et al., 2021; Fränzl et al., 2019; Jiang et al., 2020; Lin et al., 2018). Moreover, a recent study indicated that by adopting the plasmonic thermal effect (Baffou et al., 2010), one can polish the traditional optical manipulation method to a more efficient and accurate level of sub-10 nm biomolecules(Hong et al., 2020). In this study, we designed an in-situ thermophoresis-driven molecular interaction enhancement strategy for lab-on-chip applications. This, to our knowledge, is the first use of timely varying opto-thermophoresis for biomolecular manipulation and interaction enhancement. The sensitivity enhancement factor of 23.6 is the highest enhancement factor ever achieved in existing active SPRi sensing schemes. In addition, the combination of WSPRi technique here also enables 2D real-time imaging of the biomolecular binding event in the near-field region. Nevertheless, apart from SPRi sensing enhancement, we believe that this active biosensing approach can also be adopted to a wide range of surface-based sensing platforms.

2. Material and methods

The schematic of our setup is shown in Fig. 1. The system is designed into two parts: the Wavelength based surface plasmon resonance imaging (WSPRi) part below the sensor chip and the optothermal excitation part on top.

2.1. Wavelength based surface plasmon resonance imaging

For the WSPRi part, in the left arm, a halogen lamp was used as the SPR excitation light source. The broadband-spectrum light from the halogen was coupled to a multimode optical fiber (MF) through a group of lenses. The fiber light passed through a collimating lens group (L1, L2) and a pinhole; the parallel light reached the liquid crystal tunable filter (LCTF) (VariSpec, VIS-10-20-STD), which scans the output spectrum with the full width at half maximum of 10 nm and response time of 50 ms. In the experiments, the wavelength scanning range was from 610 nm to 646 nm with a scanning step of 2 nm. Then it was coupled into the prism and excites the surface plasmon wave on the surface of Au-coated sensing chip (Fabrication process is shown in S1). To monitor the combination process of antigen and antibody binding (enlarge view in Fig. 1), in the right arm, the light with sample information, after reflection by the sensing region, passed through the microscopic imaging group consisting of objective lens (10X Nikon Plan Fluorite Imaging Objective, 0.3 NA), tube lens, and the CMOS1 (Imaging, DMK33GP1300) for subsequent SPR imaging. During the experiments, the WSPRi constantly monitored all the SPR spectra on the sensing surface, and each pixel on the image of the sensor surface could produce one SPR curve, which represented the molecule binding event in the near-field region of the sensing surface. Therefore, a whole SPR hyperspectral image was obtained in real-time, and the resonance wavelength shift $\Delta\lambda$ gives us an indication about the association rate of the biomolecules on the sensing region(Zeng et al., 2019).

2.2. Optothermal excitation part

This part was designed for molecular manipulation and enrichment. Here, a laser diode of 785 nm was adopted as the heating source, controlled by a signal generator (Tektrinix, AFG1062). The laser beam was focused to a spot size of 4 μm in diameter after passing through the expander lens group (L4, L5), beam splitter (BS), and the objective lens (10X Nikon Plan Fluorite Imaging Objective, 0.3 NA). Laser power was set to 60 mW, the laser power density on the gold surface is 4.78 mW/μm^2. An image sensor CMOS2 on the top (Imaging, DMK33GP1300) was for sample visualization during testing. Two major kinds of optothermal induced thermodynamic phenomena, convective flow and thermophoresis, were excited for biomolecular enrichment and sensing. The two phenomena have greatly facilitated optical force induced tweezers (Xin et al., 2020) because of their abilities of long-range manipulation and facile energy-efficient trapping of small particles in recent years(Chen et al. 2015a, 2020; Kang et al., 2015a).

2.3. Working principle

The interaction between antibody and antigen is a complex and dynamic phenomenon based on noncovalent forces. The interaction between antibody Ab and antigen Ag at equilibrium can be expressed as (Azimzadeh and Van Regenmortel, 1990):

$$Ab + Ag \rightleftharpoons Ab - Ag$$

When antibody Ab and antigen Ag tend to combine, several criteria are required: (i) The distance between Ab and Ag is small enough (from 11.7 nm to 13.4 nm) (Sosnick et al., 1992); (ii) The two molecules must be arranged in the proper spatial orientation for effective binding. To

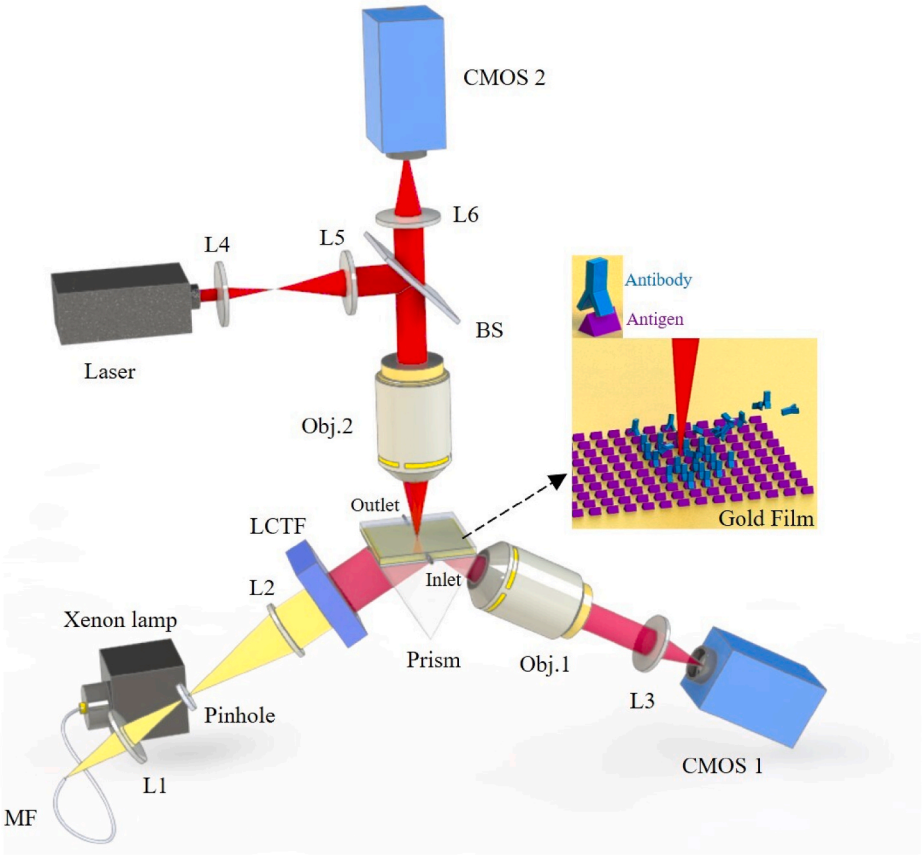

Fig. 1. Optical setup. The WSPRi part and optothermal excitation part. Lens groups of L1/L2 and L4/L5: Beam expanding and collimating; L3, L6: Tube lens; Obj.1-2: Objective lenses; MF: Multimode optical fiber; BS: Beam splitter.

promote the antibody and antigen binding event, we need to disrupt the original Brownian diffusion-limited dynamics and push the corresponding biomolecules to their counterparts to form an effective binding. Here, in the microfluidic channel with a low Reynolds number, we designed our system by simply adopting two laser excited thermodynamic forces. As the operation principle in Fig. 2 depicts, after switching on the heating laser of 785 nm, the temperature profile and the convective flow are generated, and they can be stabilized in several microseconds after laser excitation(Donner et al., 2011). The details of the temperature measurement experiment are given in S2.

There exist three dominant thermodynamic phenomena; the large-scale natural convective flow, as well as the temperature gradient dependent thermophoresis and thermo-osmotic flow. As the red arrow in Fig. 2(a) shows, in the microfluidic channel, the convective flow brings biomolecules from hundreds of micrometers away to the hottest region in a toroidal shape which is governed by Navier–Stokes

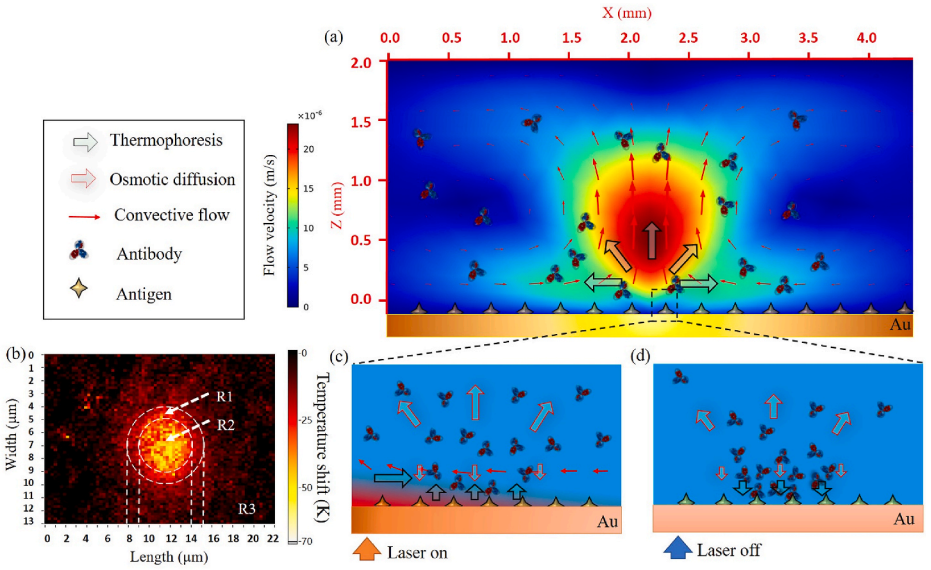

Fig. 2. Schematic illustration and theoretical analysis of OTF system. (a) Schematic side view of the entire system when the heating laser is switching on. The convective flow, which contains natural convective flow and thermo-osmotic flow, together with the thermophoresis, relocated and enriched the biomolecules from bulk solution to a ring shape region where the temperature is in relatively lower level; (b) Top view of the ring shape biomolecule aggregation region in the background of near-field temperature map. R1: ring-shape biomolecule enrichment and binding region; R2: heating laser focusing center region; R3: background region with no laser heating. (c) Zoom-in schematic picture of the biomolecule enrichment region when laser is switched on, the upward thermophoretic (UT) force induces inefficient binding of the biomolecules; (d) Zoom-in schematic picture of the biomolecule enrichment region when laser is just switched off, the flipped thermophoretic (FT) force (downward) induces efficient binding of the biomolecules.

equations, and the convective force is dominated by Stokes' law:

$$F_{CON} = 6\pi\eta R v \quad (1)$$

Where η is the viscosity coefficient, R is the hydrodynamic radius of the suspended antibody, and v is the relative velocity between the antibody and the fluid. Therefore, the biomolecules suspended in the solution are migrating in a toroidal shape convective flow cycle. Note that the flow velocity is in the micrometer per second level since the velocity profile is presented in millimeter scale landscape, the flow velocity can decrease to a level of nanometer per second near the gold surface because of the boundary effect. And all the solute and water molecules are migrating together with the biomolecules in the cycle. However, when some of the biomolecules approach the region with a higher temperature gradient (near the flow convergence center), the thermophoretic force (F_{TH}) exerted on the molecules plays a major role. Thermophoresis, which describes the drift of particles or molecules due to the temperature gradient in the solvent, is usually described by the formula:

$$v_T = -D_T \cdot \nabla \mathrm{T} \quad (2)$$

Where, v_T is the driving velocity of micro-particles or biomacromolecules in the solution, ∇T is the temperature gradient, $D_T = S_T \cdot D$ is the thermophoresis mobility, S_T is the Soret coefficient and D is the diffusion coefficient induced by Brownian motion. Although formula (2) seems quite simple, the magnitude and direction of D_T or S_T are susceptible to many parameters in the surrounding solutions and the biomolecule itself, such as the molecule's hydrodynamic size, (Braibanti et al., 2008) surface entropy, (Putnam and Cahill, 2005)' (Putnam et al., 2007) surface hydrophilicity, (Lüsebrink et al., 2012) surface charge, (Ding et al., 2020; Rasuli and Golestanian, 2008; Reichl et al., 2014; Würger, 2008) and solution ion composition and pH value.(Eslahian et al., 2014; Putnam and Cahill, 2005; Vigolo et al., 2010)

In the electrolyte solution, the thermophoretic force F_{TH} on the charged biomacromolecules governs by thermo-electrophoresis mechanism which is known as the Seebeck effect(Reichl et al., 2014). Analog to the PN junction charge diffusion, the temperature gradient can introduce redistribution of anions and cations in the solution and thus can produce a thermal-induced internal electric field that can drive the charged particles or macromolecules. A recent study gives a summary and explanation of the mechanism via molecular dynamics simulations; it indicates that a particle with negative surface charge will be driven to a cooler region in an inorganic electrolyte solution such as sodium chloride (NaCl)(Ding et al., 2020). Typically, a PBS solution (phosphate buffered saline, pH 7.4) is the most used buffer in biomedical experiments. The anions and cations in the solution are majorly Cl^- and Na^+ (The NaCL is 136 mM in commonly used 0.1 M PBS solution) as well as a small amount of phosphate. At pH = 7.4 the surface charge of most proteins, such as Immunoglobulin G (IgG) proteins, is negative (represented by Debye–Hückel–Henry charge, Z_{DHH} is ranged from 0 to – 13), (Filoti et al., 2015)' (Yang et al., 2019) which gives a positive S_T; therefore according to Equation (2), the macromolecules such as IgG protein are thermophobic and will be pushed away from the hottest laser spot center.

On the other hand, in addition to the natural convective flow circulating at millimeter scale as Fig. 2 (a) shows, when it comes to the optical nearfield region of gold surface where biomolecule interaction happens, there also exists a creep flow, named as thermo-osmotic flow, at the surface of the Au film, which is caused by the tangential temperature-gradient at the interface between the liquid solution and the solid surface(Derjaguin et al., 1987). The corresponding slip velocity is expressed as: $v_s = \chi \cdot \nabla \mathrm{T}/T$, where χ is called thermo-osmotic coefficient or mechano-caloric cross-coefficient which determines the direction of the flow. This phenomenon is characterized by the excess specific enthalpy (h) at the interface comparing to the bulk by: $\chi = -\frac{1}{\eta}\int_0^\infty z h(z) dz$. Therefore, a negative enthalpy ($h < 0$) produces a positive χ which will drive liquid towards hot site and vice versa. We can expect that the illuminated hot spot on Au film releases heat to the surrounding liquid, thus introducing a horizontal flow from cold to hot regions that will drive towards the hot spot center(Bregulla et al., 2016; Gargiulo et al., 2017). Together with thermophoresis and nature convective flow, the net force leads to the aggregation of antibodies into the ring-shaped stagnant zone on the gold surface (R1 in Fig. 2(b)), which is similar to a DNA thermal enrichment scheme with positive S_T(Braun and Libchaber, 2002). The measured near-field temperature rising in this region R1 is about 20 K; the positive S_T prevents the biomolecules from going into the laser focusing center, region R2, which has the highest temperature increment. Other forces such as optical force may also contribute to the enrichment, while it has been proven to be trivial here comparing to the thermodynamic forces in our previous studies(Chen et al., 2015a; Kang et al., 2015b).

Nevertheless, in this scenario, although the molecules (antibody) are gathered near the Au film, they cannot efficiently bind with the antigen on the Au film. Since the Au film and the glass substrate have a higher thermal conductivity and lower specific heat capacity than the bulk solution, the temperature of the Au film (T_{Au}) is higher than that of the surrounding solution (T_{So}); And the temperature difference ($\Delta T = T_{Au} - T_{So}$) is about 5 K [Fig. 3(d)]. Therefore, as the force analysis in Fig. 3(a) indicates, the aggregated molecules experience a thermophoretic force (vertical component of F_{TH}) in the upward direction that tends to push them away from the Au film. And at a certain radial distance near the laser spot edge, F_{TH} is counterbalanced by the convective dragging force F_{CON} and the particle-surface interaction force F_{PS}(Hatlo and Lue, 2008; Schein et al., 2015). Therefore, at the steady state when the laser is switching on, the antibodies can aggregate in a ring-shaped stagnant zone where the net force is zero in the vicinity of the Au film. However, because the upward F_{TH} becomes larger when the proteins are getting close to the Au surface, the proteins cannot efficiently bind with the antigens on the gold surface at this stage.

2.4. Force analysis

On the contrary, when the laser is just switched off, the thermophoretic force is flipped instantaneously in the vicinity of the sensing surface (See the thermophoretic force map in Fig. 3 (b,c)) which greatly facilitates biomolecular binding. To explain this phenomenon, we investigated the temperature data of a point in R1 region, as Fig. 3(d–f) indicate, from the very moment when the laser is switched off to a transient time about tens of microseconds afterward, the heat dissipates faster in the Au film than in the solution near the interface because of the higher thermal conductivity. The temperature in the bulk solution is higher than the Au film. The temperature gradient in z-direction (∇T_z) is reversed. While S_T remains positive, so the Z-component of the thermophoretic force F_{TH} is temporally reversed and pointing to the gold film, and the convective flow drag force F_{CON} becomes even smaller in the vicinity of the surface. Therefore, accompanied with the particle-surface interaction force F_{PS} and osmotic diffusion induced by the concentration difference, the aggregated biomolecules near the Au film are pushed to the Au film, and a higher binding rate occurs at this transient time after the heating laser is switched off. Subsequently, at laser-off status (after 100 μs), ΔT becomes trivial. While because of the diffusion, the binding events are continuing until an equilibrium stage is reached when the concentration difference is smaller.

3. Results and discussion

3.1. Particle motion monitoring

As Fig. 4 (a) shows, we conducted a qualitative experiment by using single particle tracer to track the motion of the particle motion along the z-direction as the laser is tuned ON/OFF to verify that the axial thermophoretic force is indeed flipped. The experiment is done by adopting

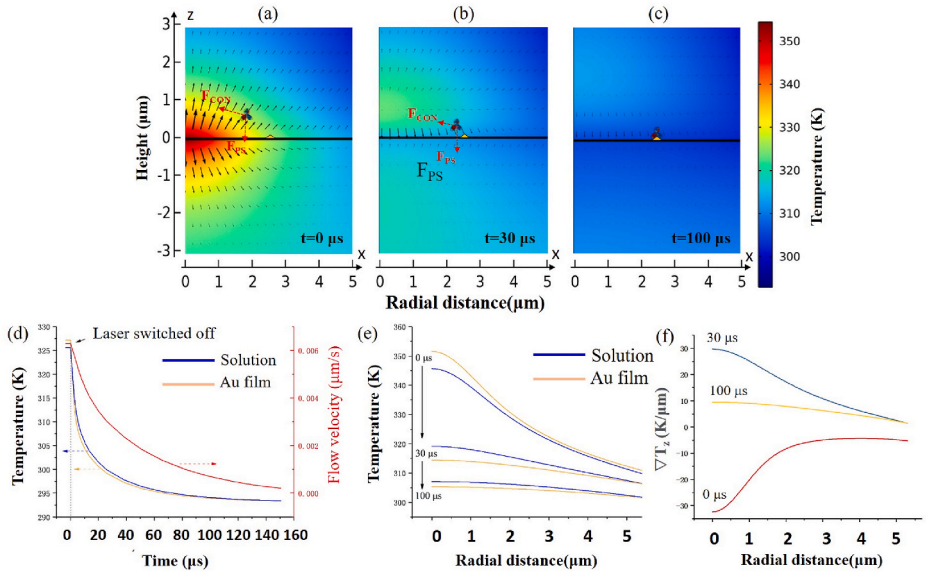

Fig. 3. Temperature distribution and force analysis in OTF antibody-antigen binding enhancement method. (a)–(c) Force arrow map due to thermophoresis in units of the negative thermophoresis mobility $-D_T$ and the temperature distribution (symmetrical half) near the laser spot at 0 μs (heating laser switched off), 30 μs, and 100 μs, respectively. F_{CON}, F_{TH} and F_{PS} are convective flow forces induced by the nature convection and thermo-osmotic flow, thermophoresis, and particle-surface interaction force respectively. (d) Temperature temporal variation comparison between the sample solution and the Au film surface as well as the convective flow velocity variation. The temperature and flow velocity interrogation point located at 2.5 μm radial distance from the laser spot center and 200 nm above the Au film. (e) Temperature and (f) temperature gradient in z-direction (∇T_z) distribution in 200 nm above the Au film. Details of the simulation are shown in S3.

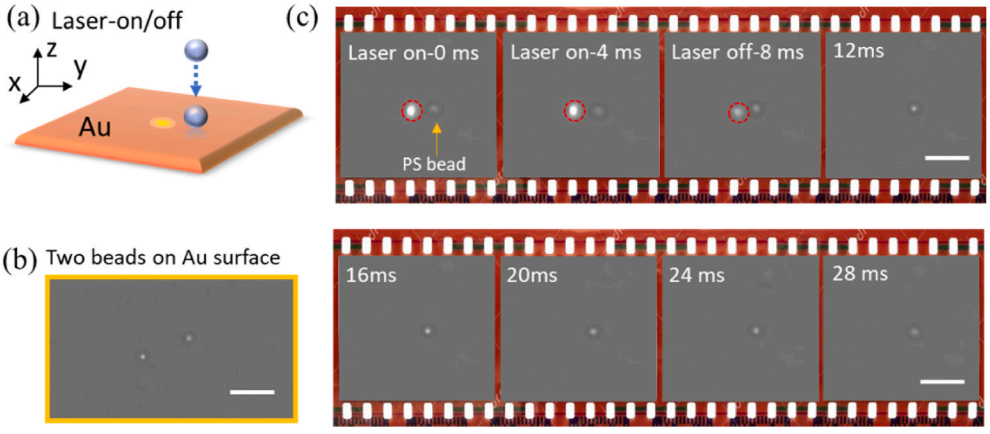

Fig. 4. Experiment of height variation of tracer particle indicated by defocusing images. (a) Configuration of the experiment that a PS bead is pushed towards to the gold surface after the heating laser is switched off. (b) The image of two PS beads attached to the gold surface at the focal plane of 100 × objective for defocusing PS bead image comparison. (c) Time-sequence images of a PS bead vertical motion driven by flipped thermophoresis right after the heating laser switched off. The dashed circular lines indicate the 785 nm laser focusing center. Scale bars: 3 μm.

the tracer particle of polystyrene (PS) bead (500 nm in diameter) with positive S_T. And an objective lens of 100 × is adopted for laser focusing and observation. And the 785 nm laser was focused to a spot of 1.26 μm in diameter and the power was adjusted to 6 mW, so power intensity (4.78 mW/μm^2) was the same as that in the OTF sensing enhancement experiment.

Comparing with the in-focusing image of the two PS beads attached to the gold surface [Fig. 4(b)], the bead motion in z-direction can be implied by recording the defocusing image of the bead. As shown in Fig. 4 (c), at laser-on status, a single PS bead near the laser focusing center will be pushed away from the focusing center because of the convection flow and upward thermophoresis, thus, it cannot reach to the surface of the gold film. While after the heating laser is switched off at t = 8 ms, because of the flipped thermophoresis, the bead immediately dives to the gold surface. The bead gradually defocuses afterward due to Brownian motion. Therefore, this experiment goes consistently with the simulation and verified the flipped thermophoresis when heating laser is switched off.

3.2. Antibody-antigen binding enhancement

We conducted an antibody-antigen binding experiment to test the biosensing enhancement ability of our method. Here we used an antibody-antigen pair of human IgG/goat-anti-human IgG. After a pre-treatment process of the sensing chip (See S4), a layer of human IgG probes was fixed on the Au film. Then 500 ng/ml goat-anti-human IgG solution (PBS buffering) was injected into the flow cell. And the binding event was monitored by the WSPRi. Note that in this level of molecule concentration, the corresponding $\Delta\lambda$ is not detectable in traditional WSPRi without the interaction enhancement (Ng et al., 2011; Wang et al., 2020). And the SPR wavelength shifting during the testing is presented in Fig. 5(a) and cycles of laser heating with on/off (120s/300s) modulation are applied on the Au film, i.e., in each cycle, the duration of laser switching on and off time was 120s and 300s, respectively. The SPR wavelength shift $\Delta\lambda$ is in positive correlation to the solution's refractive index as well as the effective binding of the goat-anti-human IgG protein(Wang et al., 2020; Zeng et al., 2016). And a rising temperature can decrease the refractive of the gold film and solution(Aly and Esmail, 1993; Chen et al., 2015b). Therefore, the SPR wavelength dropped dramatically as the heating laser was switched on.

The experimental results were consistent with our simulation. After 5 cycles of the OTF-enhanced IgG protein binding, the whole sensing site could be divided into three regions (R1-R3) as Fig. 2(b) indicates. The region R3 without heating laser treatment has no SPR wavelength shift at each cycle, and the region R2 where the laser focusing center is located had insignificant SPR wavelength shift because of the upward thermophoretic force. While the region of R1, where proteins have the aggregation and efficient binding, produces the most obvious

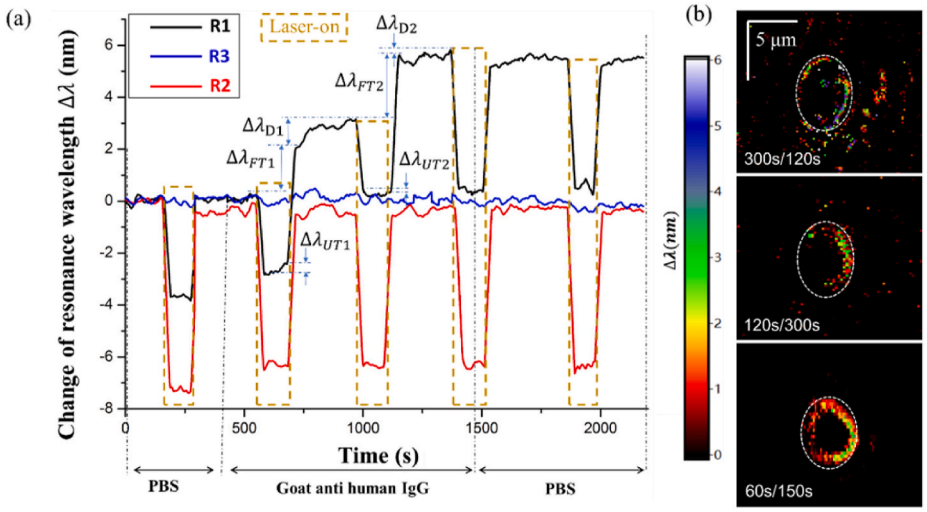

Fig. 5. Experimental demonstration of OTF-enhanced SPR imaging capabilities via binding of 0.5 μg/mL goat anti human IgG with the probes on gold surface. (a) Temporal variation of the $\Delta\lambda$ induced by the heating laser on/off modulation (120s/300s on/off period). Three curves are the resonance wavelength real-time response curves, and each point on the curve is the averaged value in the corresponding sub-regions (4 × 6 pixels) that produce the largest resonance wavelength shift from the three interrogation regions of R1, R2 and R3 in IgG binding experiments. (b) SPR image of the whole sensing site of three on/off period of 300s/120s, 120s/300s, and 60s/120s, respectively. The change of resonance wavelength $\Delta\lambda$ indicates the SPR peak shifting after the experiment.

wavelength shift.

In addition, during the heating laser illumination in each cycle, the upward thermophoretic (UT) force precludes effective binding. So, the resonance wavelength shift $\Delta\lambda_{UTi}$ (i = 1,2,3 …) at laser-on status in each cycle was quite small. When the laser was switched off, the heat in micrometer scale dissipated rapidly. The transient flipped thermophoretic (FT) force is in a downward direction, which greatly promoting the binding events. Therefore, at each rising edge of the curve, the change of resonance wavelength $\Delta\lambda_{FTi}$ (i = 1,2,3 …) induced by FT force gives the largest (1–2 nm) value in the whole modulation cycle. Subsequently, during the time without heating laser illumination, the osmotic diffusion and Brownian motion induced diffusion governed the binding event, the corresponding change of resonance wavelength $\Delta\lambda_{Di}$ (i = 1,2,3 …) was maintained at a lower level (<1 nm). Moreover, the WSPRi manifested its unique advantage of SPR wavelength imaging in this experiment; it has greatly facilitated finding the corresponding biomolecular binding region's location, shape, and concentration. As the SPR wavelength image indicates [Fig. 5(b)], the goat-anti-human IgG proteins were aggregated in a ring-shape with a horizontal radius of 2.5 μm from the heating laser focusing spot (4 μm in diameter) center.

3.3. Optimization

Moreover, although the highest binding rate was attributed to the falling edge of the heating laser modulation (laser switched off), the laser on/off duration matters, too. The modulation function can be further optimized to produce the highest biomolecular binding rate. We did a series of systematic experiments with different heating laser modulation functions. As shown in Fig. 6, the modulation functions have different duty cycles and periods. It turns out that the 120s/300s on/off period can produce the highest binding rate. In the period of laser on or off, the localized concentration of the biomolecules in the solution will gradually reach to their equilibrium stage. When the laser is on, the UT force prevents an efficient binding, the molecules in the surrounding solution need some time to form a detectable biomolecule aggregation, so that the molecules in the vicinity of the Au film can be well prepared for binding. The results have shown that 120s of laser-on time is enough for the biomolecules to form an efficient concentration enrichment

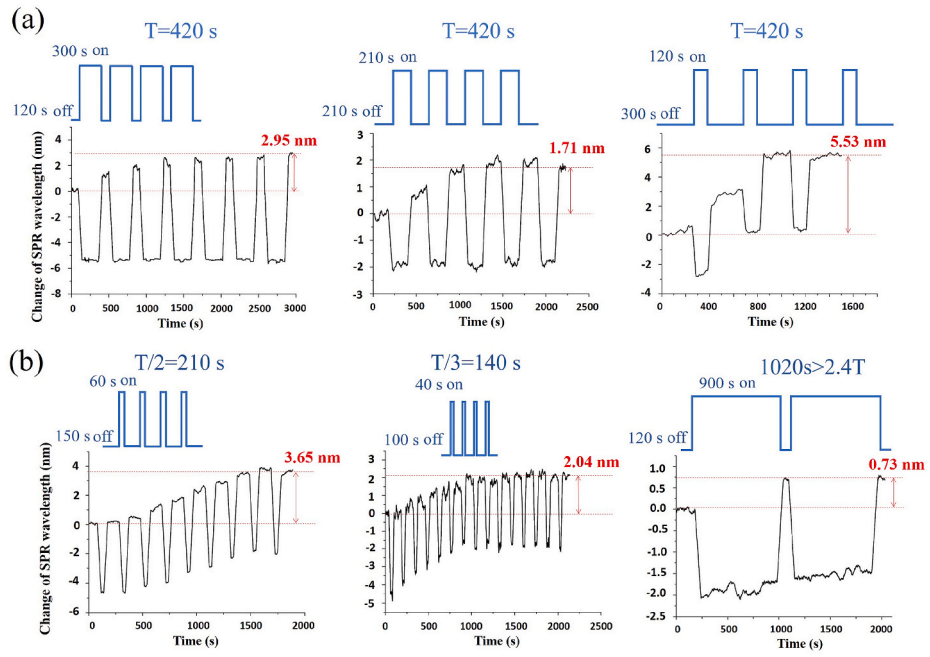

Fig. 6. Optimized heating laser on/off time investigation in goat anti human IgG (500 ng/ml). Under the heating laser power of 60 mW, a series of heating laser triggering signals (laser on/off duration) of different (a) duty cycles and (b) period T are studied. The net SPR wavelength shift after the experiments $\Delta\lambda$ are denoted in red. Each point on the curves is the averaged value of resonance wavelength change in the corresponding sub-regions of 4 × 6 pixels that produce the largest $\Delta\lambda$ from the ring-shape interrogation region R1.

region that reaches the dynamic balance. And a shorter laser-on time will induce lesser amount of molecule enrichment, and a longer time will make no further contribution to the molecule's enrichment as the equilibrium stage has already reached in 120s.

Subsequently, after concentrating an enough number of molecules in the vicinity of Au film in laser-on status, in the laser-off status, following the transient time of FT force vanishing, the binding event is governed by the osmotic force induced by the concentration gradient and the Brownian-motion diffusion. However, the diffusion is towards all directions. Therefore, it takes about 300s to reach the equilibrium where the curve is at a plateau stage, and the $\Delta\lambda_{Di}$ reaches its largest value. Noted that a longer off-status duration could not give a larger $\Delta\lambda_{Di}$, the molecules will diffuse away from the efficient binding area, which hinders the re-formation of the molecule aggregation in next cycle's on-status duration. Therefore, the optimized on/off time of heating laser is 120s/300s for getting a highest biomolecule binding rate at the laser power of 60 mW. The optimized on/off time varies from different heating laser parameters such as its wavelength or optical power density as well as the biomolecular species. The users can tune the laser modulation function and find the optimized on/off time based on experimental conditions. In addition, the resonance wavelength imaging capability also enables users to find the most sensitive sub-region that produces the largest $\Delta\lambda$.

3.4. Enhancement performance in different concentrations

In addition, we also tested the performance in different biomolecular concentrations. As Fig. 7(a) shows, a lower concentration produced a smaller $\Delta\lambda$. Simultaneously, the system's responses without using OTF were also tested. As shown in Fig. 7(b), with the assistance of OTF, the variation ratio K of SPR response $\Delta\lambda$ versus biomolecule concentration has dramatically increased by a factor of 23.6 compared to the traditional SPRi sensing scheme without using OTF. Therefore, the sensitivity enhancement factor of our system is about 23.6 $\times$, which is by far the highest sensitivity enhancement factor for the wavelength scanning type SPR imaging sensor. Moreover, the inter-biomolecular affinity varies differently in different species (Azimzadeh and Van Regenmortel, 1990); a higher association rate can produce a higher sensitivity and lower detection limit. Also, the adopted sensing platform of WSPRi is wavelength based, which cannot intrinsically produce the highest sensitivity. It is well known that the phase modes can produce the highest sensitivity among the four SPR interrogation methods of intensity, angle, wavelength, and phase modes(Law et al., 2011; Zeng et al., 2017). Therefore, the sensitivity can be further improved if the OTF method is applied in other biosensing platforms.

4. Conclusion

To tackle the difficulty of diffusion-limited biosensing, we developed, through temporal modulation of the thermophoretic force and the

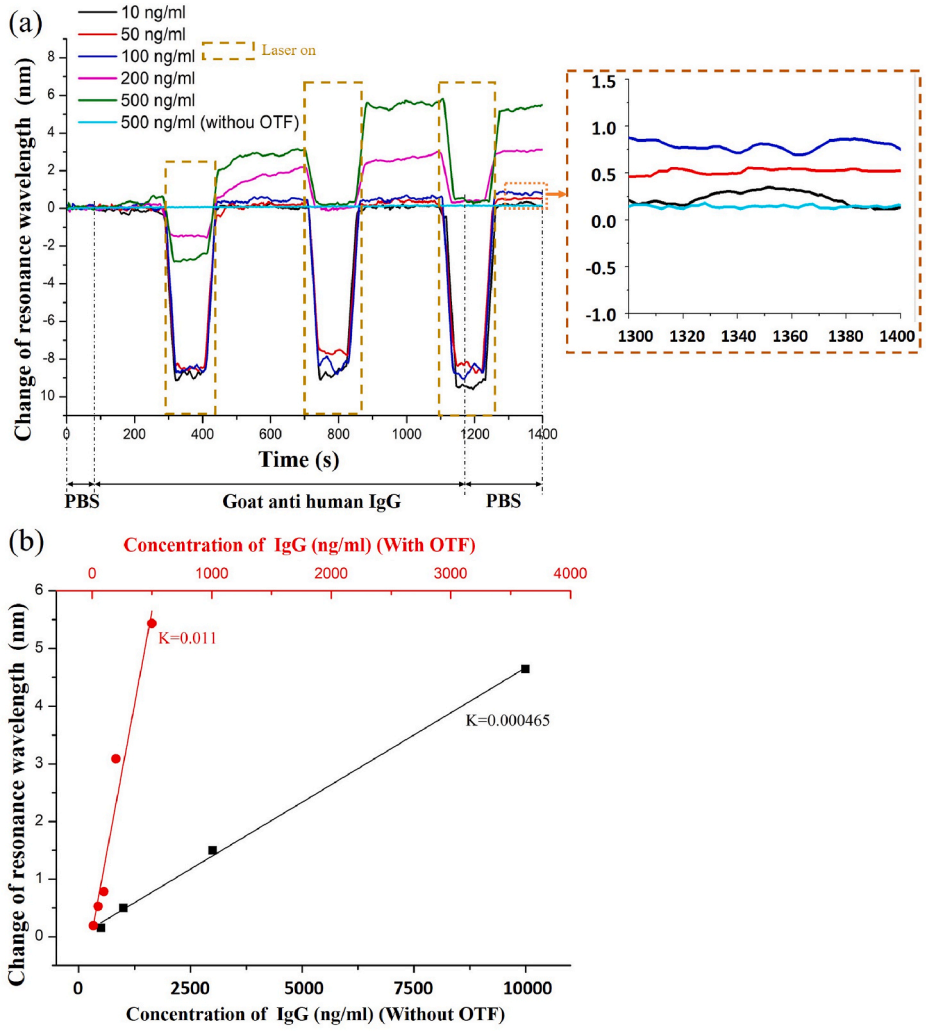

Fig. 7. The enrichment ability test for different Goat anti human IgG concentrations. (a) The change of SPR wavelength with different biomolecule concentrations during the tests. The calculated lowest concentration of biomolecule is 62.5 pM (10 ng/ml, molecular weight of Goat anti human IgG is 160 kDa). (b) Plots of terminal SPR wavelength shift $\Delta\lambda$ of different IgG concentrations with and without OTF. The red and black lines are the linear fitting of the corresponding data. The variation ratio of SPR response $\Delta\lambda$ versus biomolecule concentration is denoted as K.

convective flow, an OTF method for surface-based *in situ* protein-protein interaction enhancement. The presented OTF method is a milestone that provides multiple perspectives of using time-varying optothermal phenomena in the biomolecular manipulation and biosensing sensitivity enhancement. The all-optical approach can operate in PBS solution which is most commonly used buffer solution, so the method can be readily adopted in a wide range of biochemical studies. It functionalizes in two steps: First is the enrichment of the low concentration biomolecules to a ring-shaped aggregation, and the second step is to push the biomolecular aggregation closer to their counterparts on the Au film for enhancing the surface capture. This operation continues repeatedly until the highest interaction rate is achieved. It enables the enrichment of nanometer-scale biomolecules at a low-temperature ring-shaped region that situates several micrometers away from the hottest laser spot center. As we turned on the heating laser in each cycle, the temperature increment in the ring-shaped region R1 is 20 K, while we can still obtain the SPR wavelength shift in the next laser on/off cycles (Figs. 5–7). In addition, the PBS flushing process at the end of the experiment also verified the specific binding of the target molecules. Moreover, the change is proportional to the concentration. Therefore, at this temperature increment level, the intermolecular binding process is still functioning. More importantly, the major biomolecular interaction starts at the very moment that the heating laser is turned off and the heat dissipated rapidly in several microseconds. We believe that the influence of temperature increment on biomolecule interaction is trivial. In fact, elevated temperatures may affect the structure of antigens, but not necessarily affect the binding of antigens to antibodies since most antibodies recognize only a few peptides on the surface of the antigen. As in the western blotting experiment for specific protein (antibody/antigen) identification (Mahmood and Yang, 2012), the proteins are boiled in 100 °C and denatured, and they can still effectively bind to the antibody on the membrane. Moreover, the real-time imaging ability of surface plasmon resonance imaging (WSPRi) makes it easy to locate the most responsive region of the biomolecular interactions, and one can randomly choose and manipulate the region of interest for sensing. Thus, we have achieved an enhancement factor of 23.6. This, to our knowledge, is the highest enhancement factor that has ever been achieved in existing active SPR sensing schemes. This is also the first time that the dynamic transient heating dissipation process is adopted for biomolecular manipulation in lab-on-a-chip platforms. In addition, OTF is a promising tool for biological sensing of analytes at low levels. It can concentrate biological molecules at picomolar concentrations within a few minutes, and it can be applied to a wide range of biomolecular manipulations since most of them have positive S_T. Furthermore, the method can potentially obtain a further improved sensitivity and detection limit if it is applied on other sensing platforms or carrying out biomolecular manipulations of other kinds. In conclusion, the present work opens a new epoch in widespread applications in microfluidic biosensing platforms when ultrahigh sensitivity is necessary. We believe that it can also promote the development of a wider range of scientific and clinical applications in biological studies.

CRediT authorship contribution statement

Jiajie Chen: Conceptualization, Methodology, Data curation, Writing – original draft, Funding acquisition, Supervision. **Youjun Zeng:** Investigation, Methodology, Data curation, Writing – original draft. **Jie Zhou:** Investigation, Methodology. **Xueliang Wang:** Investigation, Software. **Boliang Jia:** Investigation, Methodology. **Ruibiao Miyan:** Methodology. **Teliang Zhang:** Methodology. **Wei Sang:** Methodology. **Ying Wang:** Investigation. **Haixia Qiu:** Investigation. **Junle Qu:** Investigation, Supervision. **Ho-Pui Ho:** Investigation. **Bruce Zhi Gao:** Writing – review & editing. **Yonghong Shao:** Writing – review & editing, Project administration, Funding acquisition, Supervision. **Ying Gu:** Funding acquisition, Supervision.

Declaration of competing interest

The authors declare that they have no known competing financial interests or personal relationships that could have appeared to influence the work reported in this paper.

Acknowledgments

This work was supported by the Project from National Natural Science Foundation of China (61905145, 61775148, and 61527827); National Key Research and Development Program of China (2017YFB0403804); Guangdong Natural Science Foundation and Province Project (2021A1515011916, 2018A030310544); Shenzhen Science and Technology R&D and Innovation Foundation (JCYJ20180305124754860, JCYJ20200109105608771).

Appendix A. Supplementary data

Supplementary data to this article can be found online at https://doi.org/10.1016/j.bios.2022.114084.

References

Aly, K.M., Esmail, E., 1993. Refractive index of salt water: effect of temperature. Opt. Mater. 2 (3), 195–199.
Azimzadeh, A., Van Regenmortel, M., 1990. Antibody affinity measurements. J. Mol. Recogn. 3 (3), 108–116.
Baffou, G., Quidant, R., García de Abajo, F.J., 2010. Nanoscale control of optical heating in complex plasmonic systems. ACS Nano 4 (2), 709–716.
Barik, A., Zhang, Y., Grassi, R., Nadappuram, B.P., Edel, J.B., Low, T., Koester, S.J., Oh, S.-H., 2017. Graphene-edge dielectrophoretic tweezers for trapping of biomolecules. Nat. Commun. 8 (1), 1867.
Braibanti, M., Vigolo, D., Piazza, R., 2008. Does thermophoretic mobility depend on particle size? Phys. Rev. Lett. 100 (10), 108303.
Brangel, P., Sobarzo, A., Parolo, C., Miller, B.S., Howes, P.D., Gelkop, S., Lutwama, J.J., Dye, J.M., McKendry, R.A., Lobel, L., 2018. A serological point-of-care test for the detection of IgG antibodies against Ebola virus in human survivors. ACS Nano 12 (1), 63–73.
Braun, D., Libchaber, A., 2002. Trapping of DNA by thermophoretic depletion and convection. Phys. Rev. Lett. 89 (18), 188103.
Braun, M., Cichos, F., 2013. Optically controlled thermophoretic trapping of single nano-objects. ACS Nano 7 (12), 11200–11208.
Bregulla, A.P., Würger, A., Günther, K., Mertig, M., Cichos, F., 2016. Thermo-osmotic flow in thin films. Phys. Rev. Lett. 116 (18), 188303.
Chen, J., Cong, H., Loo, F.-C., Kang, Z., Tang, M., Zhang, H., Wu, S.-Y., Kong, S.-K., Ho, H.-P., 2016a. Thermal gradient induced tweezers for the manipulation of particles and cells. Sci. Rep. 6 (1), 1–13.
Chen, J., Kang, Z., Kong, S.K., Ho, H.-P., 2015a. Plasmonic random nanostructures on fiber tip for trapping live cells and colloidal particles. Opt. Lett. 40 (17), 3926–3929.
Chen, J., Loo, J.F.C., Wang, D., Zhang, Y., Kong, S.K., Ho, H.P., 2020. Thermal optofluidics: principles and applications. Adv. Opt. Mater. 8 (1), 1900829.
Chen, K., Zeng, Y., Wang, L., Gu, D., He, J., Wu, S.-Y., Ho, H.-P., Li, X., Qu, J., Gao, B.Z., 2016b. Fast spectral surface plasmon resonance imaging sensor for real-time high-throughput detection of biomolecular interactions. J. Biomed. Opt. 21 (12), 127003.
Chen, Z.-H., Shi, H., Wang, Y., Yang, Y., Liu, S., Ye, H., 2017. Sharp convex gold grooves for fluorescence enhancement in micro/nano fluidic biosensing. J. Mater. Chem. B 5 (44), 8839–8844.
Chen, Z., Shan, X., Guan, Y., Wang, S., Zhu, J.-J., Tao, N., 2015b. Imaging local heating and thermal diffusion of nanomaterials with plasmonic thermal microscopy. ACS Nano 9 (12), 11574–11581.
Chou, I.-H., Benford, M., Beier, H.T., Coté, G.L., Wang, M., Jing, N., Kameoka, J., Good, T.A., 2008. Nanofluidic biosensing for β-amyloid detection using surface enhanced Raman spectroscopy. Nano Lett. 8 (6), 1729–1735.
Cong, H., Chen, J., Ho, H.-P., 2018. Trapping, sorting and transferring of micro-particles and live cells using electric current-induced thermal tweezers. Sensor. Actuator. B Chem. 264, 224–233.
De Angelis, F., Gentile, F., Mecarini, F., Das, G., Moretti, M., Candeloro, P., Coluccio, M., Cojoc, G., Accardo, A., Liberale, C., 2011. Breaking the diffusion limit with super-hydrophobic delivery of molecules to plasmonic nanofocusing SERS structures. Nat. Photonics 5 (11), 682–687.
Derjaguin, B.V., Churaev, N.V., Muller, V.M., Kisin, V., 1987. Surface Forces. Springer.
Ding, H., Kollipara, P.S., Lin, L., Zheng, Y., 2020. Atomistic modeling and rational design of optothermal tweezers for targeted applications. Nano Res. 14 (1), 295–303.
Ding, H., Kollipara, P.S., Lin, L., Zheng, Y., 2021. Atomistic modeling and rational design of optothermal tweezers for targeted applications. Nano Res. 14 (1), 295–303.
Donner, J.S., Baffou, G., McCloskey, D., Quidant, R., 2011. Plasmon-assisted optofluidics. ACS Nano 5 (7), 5457–5462.
Dufour, D.R., Talastas, M., Fernandez, M.D., Harris, B., 2003. Chemiluminescence assay improves specificity of hepatitis C antibody detection. Clin. Chem. 49 (6), 940–944.

Eslahian, K.A., Majee, A., Maskos, M., Würger, A., 2014. Specific salt effects on thermophoresis of charged colloids. Soft Matter 10 (12), 1931–1936.
Filoti, D.I., Shire, S.J., Yadav, S., Laue, T.M., 2015. Comparative study of analytical techniques for determining protein charge. J. Pharmaceut. Sci. 104 (7), 2123–2131.
Fränzl, M., Thalheim, T., Adler, J., Huster, D., Posseckardt, J., Mertig, M., Cichos, F., 2019. Thermophoretic trap for single amyloid fibril and protein aggregation studies. Nat. Methods 16 (7), 611–614.
Garcia-Guirado, J., Rica, R.l.A., Ortega, J., Medina, J., Sanz, V., Ruiz-Reina, E., Quidant, R., 2018. Overcoming diffusion-limited biosensing by electrothermoplasmonics. ACS Photonics 5 (9), 3673–3679.
Gargiulo, J., Brick, T., Violi, I.L., Herrera, F.C., Shibanuma, T., Albella, P., Requejo, F.G., Cortés, E., Maier, S.A., Stefani, F.D., 2017. Understanding and reducing photothermal forces for the fabrication of Au nanoparticle dimers by optical printing. Nano Lett. 17 (9), 5747–5755.
Hatlo, M.M., Lue, L., 2008. The role of image charges in the interactions between colloidal particles. Soft Matter 4 (8), 1582–1596.
Henry, A.-I., Sharma, B., Cardinal, M.F., Kurouski, D., Van Duyne, R.P., 2016. Surface-enhanced Raman spectroscopy biosensing: in vivo diagnostics and multimodal imaging. Anal. Chem. 88 (13), 6638–6647.
Hong, C., Yang, S., Ndukaife, J.C., 2020. Stand-off trapping and manipulation of sub-10 nm objects and biomolecules using opto-thermo-electrohydrodynamic tweezers. Nat. Nanotechnol. 15 (11), 908–913.
Jiang, Q., Rogez, B., Claude, J.-B., Baffou, G., Wenger, J., 2020. Quantifying the role of the surfactant and the thermophoretic force in plasmonic nano-optical trapping. Nano Lett. 20 (12), 8811–8817.
Ju, H., Yan, G., Chen, F., Chen, H., 1999. Enzyme-linked immunoassay of α-1-fetoprotein in serum by differential pulse voltammetry. Electroanalysis Int. J. Devoted Fund. Practical Aspect. Electroanalysis 11 (2), 124–128.
Kang, Z., Chen, J., Wu, S.-Y., Chen, K., Kong, S.-K., Yong, K.-T., Ho, H.-P., 2015a. Trapping and assembling of particles and live cells on large-scale random gold nano-island substrates. Sci. Rep. 5.
Kang, Z., Chen, J., Wu, S.-Y., Ho, H.-P., 2015b. Plasmonic absorption activated trapping and assembling of colloidal crystals with non-resonant continuous gold films. RSC Adv. 5 (127), 105409–105415.
Karim, F., Vasquez, E.S., Sun, Y., Zhao, C., 2019. Optothermal microbubble assisted manufacturing of nanogap-rich structures for active chemical sensing. Nanoscale 11 (43), 20589–20597.
Kim, Y., Ding, H., Zheng, Y., 2020. Enhancing surface capture and sensing of proteins with low-power optothermal bubbles in a biphasic liquid. Nano Lett. 20 (10), 7020–7027.
Lüsebrink, D., Yang, M., Ripoll, M., 2012. Thermophoresis of colloids by mesoscale simulations. J. Phys. Condens. Matter 24 (28), 284132.
Laing, S., Jamieson, L.E., Faulds, K., Graham, D., 2017. Surface-enhanced Raman spectroscopy for in vivo biosensing. Nat. Rev. Chem. 1 (8), 1–19.
Law, W.-C., Yong, K.-T., Baev, A., Hu, R., Prasad, P.N., 2009. Nanoparticle enhanced surface plasmon resonance biosensing: application of gold nanorods. Opt Express 17 (21), 19041–19046.
Law, W.-C., Yong, K.-T., Baev, A., Prasad, P.N., 2011. Sensitivity improved surface plasmon resonance biosensor for cancer biomarker detection based on plasmonic enhancement. ACS Nano 5 (6), 4858–4864.
Lequin, R.M., 2005. Enzyme immunoassay (EIA)/enzyme-linked immunosorbent assay (ELISA). Clin. Chem. 51 (12), 2415–2418.
Li, H., Shi, W., Song, J., Jang, H.-J., Dailey, J., Yu, J., Katz, H.E., 2018. Chemical and biomolecule sensing with organic field-effect transistors. Chem. Rev. 119 (1), 3–35.
Li, J., Zhu, J.-J., 2013. Quantum dots for fluorescent biosensing and bio-imaging applications. Analyst 138 (9), 2506–2515.
Liedberg, B., Lundström, I., Stenberg, E., 1993. Principles of biosensing with an extended coupling matrix and surface plasmon resonance. Sensor. Actuator. B Chem. 11 (1–3), 63–72.
Lin, L., Wang, M., Peng, X., Lissek, E.N., Mao, Z., Scarabelli, L., Adkins, E., Coskun, S., Unalan, H.E., Korgel, B.A., 2018. Opto-thermoelectric nanotweezers. Nat. Photonics 12 (4), 195–201.
Liu, R.H., Lenigk, R., Druyor-Sanchez, R.L., Yang, J., Grodzinski, P., 2003. Hybridization enhancement using cavitation microstreaming. Anal. Chem. 75 (8), 1911–1917.
Liu, X., Yang, K., Wadhwa, A., Eda, S., Li, S., Wu, J., 2011. Development of an AC electrokinetics-based immunoassay system for on-site serodiagnosis of infectious diseases. Sensor Actuator Phys. 171 (2), 406–413.
Lynn Jr., N.S., Martínez-López, J.-I., Bocková, M., Adam, P., Coello, V., Siller, H.R., Homola, J., 2014. Biosensing enhancement using passive mixing structures for microarray-based sensors. Biosens. Bioelectron. 54, 506–514.
Mahmood, T., Yang, P.-C., 2012. Western blot: technique, theory, and trouble shooting. N. Am. J. Med. Sci. 4 (9), 429.
Mejía-Salazar, J., Oliveira Jr., O.N., 2018. Plasmonic biosensing: focus review. Chem. Rev. 118 (20), 10617–10625.
Ng, S.P., Wu, C.M.L., Wu, S.Y., Ho, H.P., 2011. White-light spectral interferometry for surface plasmon resonance sensing applications. Opt Express 19 (5), 4521–4527.
Ozcelik, A., Rufo, J., Guo, F., Gu, Y., Li, P., Lata, J., Huang, T.J., 2018. Acoustic tweezers for the life sciences. Nat. Methods 15 (12), 1021–1028.
Putnam, S.A., Cahill, D.G., 2005. Transport of nanoscale latex spheres in a temperature gradient. Langmuir 21 (12), 5317–5323.
Putnam, S.A., Cahill, D.G., Wong, G.C., 2007. Temperature dependence of thermodiffusion in aqueous suspensions of charged nanoparticles. Langmuir 23 (18), 9221–9228.
Rasuli, S.N., Golestanian, R., 2008. Soret motion of a charged spherical colloid. Phys. Rev. Lett. 101 (10), 108301.
Reichl, M., Herzog, M., Götz, A., Braun, D., 2014. Why charged molecules move across a temperature gradient: the role of electric fields. Phys. Rev. Lett. 112 (19), 198101.
Schein, P., Kang, P., O'Dell, D., Erickson, D., 2015. Nanophotonic force microscopy: characterizing particle–surface interactions using near-field photonics. Nano Lett. 15 (2), 1414–1420.
Sereda, A., Moreau, J., Canva, M., Maillart, E., 2014. High performance multi-spectral interrogation for surface plasmon resonance imaging sensors. Biosens. Bioelectron. 54, 175–180.
Song, Y., Wei, W., Qu, X., 2011. Colorimetric biosensing using smart materials. Adv. Mater. 23 (37), 4215–4236.
Sosnick, T., Benjamin, D., Novotny, J., Seeger, P., Trewhella, J., 1992. Distances between the antigen-binding sites of three murine antibody subclasses measured using neutron and X-ray scattering. Biochemistry 31 (6), 1779–1786.
Sun, W., Jiao, K., Zhang, S., Zhang, C., Zhang, Z., 2001. Electrochemical detection for horseradish peroxidase-based enzyme immunoassay using p-aminophenol as substrate and its application in detection of plant virus. Anal. Chim. Acta 434 (1), 43–50.
Tanaka, T., Matsunaga, T., 2000. Fully automated chemiluminescence immunoassay of insulin using antibody– protein A– bacterial magnetic particle complexes. Anal. Chem. 72 (15), 3518–3522.
Tripp, R.A., Dluhy, R.A., Zhao, Y., 2008. Novel nanostructures for SERS biosensing. Nano Today 3 (3–4), 31–37.
Vigolo, D., Buzzaccaro, S., Piazza, R., 2010. Thermophoresis and thermoelectricity in surfactant solutions. Langmuir 26 (11), 7792–7801.
Voiculescu, I., Nordin, A.N., 2012. Acoustic wave based MEMS devices for biosensing applications. Biosens. Bioelectron. 33 (1), 1–9.
Würger, A., 2008. Transport in charged colloids driven by thermoelectricity. Phys. Rev. Lett. 101 (10), 108302.
Wang, J., 2006. Electrochemical biosensors: towards point-of-care cancer diagnostics. Biosens. Bioelectron. 21 (10), 1887–1892.
Wang, X., Zeng, Y., Zhou, J., Chen, J., Miyan, R., Zhang, H., Qu, J., Ho, H.-P., Gao, B.Z., Shao, Y., 2020. Ultrafast surface plasmon resonance imaging sensor via the high-precision four-parameter-based spectral curve readjusting method. Anal. Chem. 93 (2), 828–833.
Wu, L., Guo, J., Dai, X., Xiang, Y., Fan, D., 2018. Sensitivity enhanced by MoS 2–graphene hybrid structure in guided-wave surface plasmon resonance biosensor. Plasmonics 13 (1), 281–285.
Xin, H., Li, Y., Liu, Y.C., Zhang, Y., Xiao, Y.F., Li, B., 2020. Optical forces: from fundamental to biological applications. Adv. Mater. 32 (37), 2001994.
Xin, H., Namgung, B., Lee, L.P., 2018. Nanoplasmonic optical antennas for life sciences and medicine. Nat. Rev. Mater. 3 (8), 228–243.
Xin, H., Sim, W.J., Namgung, B., Choi, Y., Li, B., Lee, L.P., 2019. Quantum biological tunnel junction for electron transfer imaging in live cells. Nat. Commun. 10 (1), 1–11.
Yang, D., Kroe-Barrett, R., Singh, S., Laue, T., 2019. IgG charge: practical and biological implications. Antibodies 8 (1), 24.
Yuk, J.S., Jung, S.H., Jung, J.W., Hong, D.G., Han, J.A., Kim, Y.M., Ha, K.S., 2004. Analysis of protein interactions on protein arrays by a wavelength interrogation-based surface plasmon resonance biosensor. Proteomics 4 (11), 3468–3476.
Zeng, Y., Hu, R., Wang, L., Gu, D., He, J., Wu, S.-Y., Ho, H.-P., Li, X., Qu, J., Gao, B.Z., 2017. Recent advances in surface plasmon resonance imaging: detection speed, sensitivity, and portability. Nanophotonics 6 (5), 1017–1030.
Zeng, Y., Wang, L., Wu, S.-Y., He, J., Qu, J., Li, X., Ho, H.-P., Gu, D., Gao, B.Z., Shao, Y., 2016. High-throughput imaging surface plasmon resonance biosensing based on an adaptive spectral-dip tracking scheme. Opt Express 24 (25), 28303–28311.
Zeng, Y., Wang, X., Zhou, J., Miyan, R., Qu, J., Ho, H.-P., Zhou, K., Gao, B.Z., Chen, J., Shao, Y., 2020. High-throughput imaging surface plasmon resonance biosensing based on ultrafast two-point spectral-dip tracking scheme. Opt Express 28 (14), 20624–20633.
Zeng, Y., Zhou, J., Wang, X., Cai, Z., Shao, Y., 2019. Wavelength-scanning surface plasmon resonance microscopy: a novel tool for real time sensing of cell-substrate interactions. Biosens. Bioelectron. 145, 111717.
Zhang, C., Yuan, Y., Zhang, S., Wang, Y., Liu, Z., 2011. Biosensing platform based on fluorescence resonance energy transfer from upconverting nanocrystals to graphene oxide. Angew. Chem. Int. Ed. 50 (30), 6851–6854.
Zhong, W., 2009. Nanomaterials in fluorescence-based biosensing. Anal. Bioanal. Chem. 394 (1), 47–59.
Zhou, J., Zeng, Y., Wang, X., Wu, C., Cai, Z., Gao, B.Z., Gu, D., Shao, Y., 2020. The capture of antibodies by antibody-binding proteins for ABO blood typing using SPR imaging-based sensing technology. Sensor. Actuator. B Chem. 304, 127391.